Biomass Conversion and Biorefinery (2025) 15:10075–10088
https://doi.org/10.1007/s13399-024-05844-3

ORIGINAL ARTICLE

Converting lignocellulosic biomass into mesoporous carbons for the assessment of single adsorption equilibrium: the competing role of moisture and temperature on gaseous benzene adsorption

Kaan Isinkaralar[1]

Received: 13 March 2024 / Revised: 21 May 2024 / Accepted: 30 May 2024 / Published online: 25 June 2024

Abstract
For the present study, the activated carbon were obtained from *Lotus corniculatus* L. as waste biomass using carbonization at 700 °C and alkali potassium hydroxide (KOH) chemical activation technique. Single gaseous benzene (C_6H_6) adsorption (SGBA) experiments were performed to benchmark the efficiency of the *L. corniculatus*-derived activated carbons (LCACs), which were LCAC2 (609 m^2 g^{-1}, KOH 1:2 w/w), LCAC3 (742 m^2 g^{-1}, KOH 1:3 w/w), and LCAC4 (826 m^2 g^{-1}, KOH 1:4 w/w), respectively. Also, the physicochemical properties of LCACs were characterized by Fourier Transform Infrared Spectroscopy (FT-IR), thermogravimetric analysis (TGA), scanning electron microscopy (SEM), and proximate-elemental assessment. The isotherm models (Langmuir and Freundlich) of C_6H_6 demonstrate the complex adaptation results of LCAC4 at different relative humidity (RH) levels, and Freundlich isotherm is highly suitable to C_6H_6/LCAC4 as multilayer adsorption. Kinetic behavior was also analyzed and showed that of C_6H_6 is well illustrated by the pseudo second order (PSOM). The C_6H_6 competitive adsorption of LCAC2, LCAC3, and LCAC4 at 25 °C + 0 RH%, 25 °C + 80 RH%, 45 °C + 0 RH%, and 45 °C + 80 RH% corresponds to reductions of 12.9–11.6%, 7.8–11.5%, and 9.9–18.4%. The LCAC4 is confirmed to be a perfect adsorbent in the elimination of a single gaseous stream at 45 °C + 0 RH%. Regeneration showed that the LCAC4 maintained more than 25% of the initial adsorption capacity after five repeated adsorption–desorption cycles. The promising properties of LCAC4 are recommended to be exploited for the other volatile organic compounds in the gas phase in indoor environments, under the best conditions.

Keywords Adsorption mechanism · Biomass processing · Enhanced capture · Sustainable carbonaceous material · Toxic vapor

1 Introduction

Air pollution with various chemicals, including gas emissions, both biogenic (volcanoes and forest fires) and anthropogenic (crude oil, gasoline, and industrial process), has caused the formation of large quantities of volatile organic compounds (VOCs) [1]. Indoor Air Quality (IAQ) has been affected by building materials that transmit and distribute VOCs [2], which originate from indoor contaminants [3] and are defined as concern organic compounds based on the United States Environmental Protection Agency [4]. The agencies generally indicate a vapor pressure of 0.01 kPa at 19.85 °C [5] and larger than 0.0133 kPa at 24.85 °C [6]. These pollutants, with respect to their low boiling points, create severe risks to the environment and human well-being worldwide, by World Health Organization [7], very volatile (< 0 to 50–100 °C), semi-volatile (240–260 °C to 380–400 °C), and VOCs (~ 50 to 260 °C). They are dispersed throughout the ambient atmosphere by various forms of aromatic hydrocarbons (AHs), halogenated organic compounds (HOCs), organic alcohols (OAs), saturated/unsaturated hydrocarbons (SHs/USHs), and sulfur compounds (SCs) [8, 9]. Besides them, organic compounds such as benzene (C_6H_6, molecular weight: 78.11 g mol^{-1}, lifetime: few hours, with a sweet odor level of 4.785 mg m^{-3}) [10], which demand special attention in the vapor phase in the ambient air due to their toxicity, persistence, bioaccumulation,

✉ Kaan Isinkaralar
kisinkaralar@kastamonu.edu.tr

[1] Department of Environmental Engineering, Faculty of Engineering and Architecture, Kastamonu University, Kastamonu 37150, Türkiye

categorized within human carcinogens [11], and exposures via oral as well as inhalation [12]. It is largely found that their level is significantly high in some sectors, including plastics-synthetic fibers/products, resin synthesis, rubber blends, dye solution, synthetic detergent, drug design, pesticide factories, and cigarette smoke [13]. These sources can be more effective with increased ambient temperature in indoor air and an annual limit value of 5 μg m^{-3} prescribed in European Union Directive 2008/50/EC on outdoor air quality [14]. Therefore, removing benzene from gaseous waste is crucial to preserve public health and the surrounding communities.

Several methods for vapor benzene removal, such as catalytic oxidation [15], membrane technology [16], catalysts [17], photocatalysis [18], non-thermal plasma oxidation [19], and adsorption [20], have been introduced. Amongst, adsorption is considered as one of the highly attractive and cost-effective processes, due to its simplicity, efficiency, low cost, and recyclability of the adsorbent. Indeed, adsorption technology treats air control management using a medium that adsorbs gas-phase substances. Materials are referred to as adsorbents and range in composition, structure, texture and their application. Some widespread examples of adsorbents are biochar [21], activated carbons (ACs) [22], silica gel [23], polymers [24], carbon composite [25], zeolites [26], and resins [27]. Among them, activated carbon (AC) is commonly recognized as an efficient adsorbent for VOC remediation due to its relatively higher surface area, permeability, and sorption capability [28, 29]. Many scholars have applied chemically produced activated carbon to optimize the production of AC by waste lignin material [30]. Obtained AC samples have high surface area and showed excellent performance in removing several VOCs from the gaseous phase under different humidities, temperature, etc., with several removal efficiencies for pre-equilibrium adsorption assays. However, a better understanding of the adsorption mechanisms underlying this performance is fundamental, and kinetics is a key metric in characterizing adsorption processes [31]; identifying the uptake rate, it provides information on the adsorption mechanism, surface reactions, mass transfer and diffusion of the adsorbate in the process [32]. The adsorption isotherms are valuable and show the equilibrium interaction between the adsorbate molecules and the adsorbent [33], which represents the maximum adsorption capacity (MAC) possibility, as it reflects the nature and intensity of adsorbate-adsorbent reactions [34, 35]. Operational data can better clarify adsorption mechanisms, including dosage impacts, desorption studies, post-adsorption experiments, and surface chemistry analyses [36].

Unfortunately, AC is typically sourced from non-renewable materials such as coal and petroleum coke, which are costly and create significant environmental issues. Hence, there is increasing attention to improve AC from biomass materials that are both renewable and low-cost, such as organic residues [37, 38]. One of such material is lignocellulosic waste material, an agricultural residual that has a high carbon content which *Lotus corniculatus* L. (bird's foot trefoil) (Fabeaceae) plants are considered good candidates for waste biomass use and recycling to activated carbon production in our study. It spontaneously grows in various natural habitats and remains idle in the environment.

This paper mainly aims to synthesize and qualify ACs from *Lotus corniculatus* (LC) as a precursor for the single gaseous benzene adsorption (SGBA), since benzene is partly chosen as a model contaminant because of its widely utilization in indoor air and its negative effects on human, if released into the indoor environment without treatment. The LCACs were adequately evaluated by Brunauer–Emmett–Teller (BET), Fourier Transform Infrared Spectroscopy (FT-IR), Laser Raman Spectrophotometer, N_2 adsorption/desorption, Scanning Electron Microscopy (SEM), and Thermo-gravimetric analysis (TGA). The adsorption capacities of several LCACs from benzene vapor were studied, namely, as LCAC2, LCAC3, and LCAC4, which has become an attractive strategy for a comparison of the solid binding force of benzene molecules. Also, we investigated the adsorption kinetics, isotherms, and behavior of SGBA by LCAC4, addressing (i) the lack of comprehensive understanding of the adsorption processes and mechanisms pathways of benzene removal by LCAC4, (ii) comparison of the adsorption performance of LCAC4 under experimental design parameters, (iii) the regeneration capacity of LCAC4 were employed. This paper not only reveals excellent perspectives for the treatment of benzene molecules but also indicates the prospective application of LCACs for indoor air pollution control.

2 Experimental section

2.1 Materials

Lotus corniculatus L. (*Fabaceae*) waste biomass (LCB) was acquired from Kastamonu, Türkiye, and it was used in this study as a precursor. The potassium hydroxide (KOH, 99.99%) was supplied from Merck; benzene (C_6H_6, 99.8%) was purchased from Sigma-Aldrich. The experiments were conducted by nitrogen (N_2) ≥ 99.9% and distilled water having a conductivity < 1 μS cm^{-1} and chemicals were applied as purchased. The 0.1 M HCl solution was used for pH adjustments, using the analytical-grade materials purchased from Merck.

2.2 Preparation of porous carbons

The manufacturing of activated carbons (LCACs) was carried out in two major phases: (i) preparation of LCBs for synthesis and (ii) chemical activation processing. The LCBs implemented sequentially as follows: (i) resized down to about 1 × 1 cm, (ii) rinsed in distilled water, (iii) dried at 55 °C for seven days, (iv) grounded with milling, (v) sieved with 60-mesh, and (vi) powdered LCB was mixed with KOH impregnation weight ratio (IWR) of 1:2, 1:3, and 1:4 w/w, which can destroy the carbon layer structure of LCB. They were stirred until paste at 180 °C for 2 h. Dry blend was received in a high-temperature resistant tube reactor, including horizontal tubular furnace, under the (N_2) flow at a 110 mL/min flow rate and activated at 700 °C for 2 h. After carbonization, the produced blend cooled down, was washed several times with 0.1 M HCl, and was rinsed with distilled water until the pH was roughly ~7. They were separated using a 0.45 µm filter and were dried at 105 °C for 48 h. Eventually, the LCACs were labeled appropriately in Table 1.

2.3 Textural characterization of LCACs

N_2 adsorption/desorption isotherms were used to evaluate the porous structure of LCACs, and it is specified at − 196 °C by an Autosorb-1-C (Quantachrome Instruments, United States). The Brunauer–Emmett–Teller (BET) equation was applied to predict the surface area (S_{BET} m^2 g^{-1}) and to define the total pore volume (V_T cm^3 g^{-1}). They were obtained by properly matching the liquid volumes of N_2 to the number adsorbed at a relative high pressure (P/P_0 of 0.99) [39]. The micropore volume (V_μ cm^3 g^{-1}) was obtained by the Dubinin-Radushkevich (DR) equation, and the mesopore volume (V_m cm^3 g^{-1}) was considered as the space between V_T and V_μ cm^3 g^{-1} [40]. The average pore diameter (d_p nm) was determined by the equation $d_p = 4V_T/S_{BET}$. The pore size distribution of the LCACs was described by Barrett–Joyner–Halenda (BJH) method [41]. The surface morphology of LCACs was characterized under argon conditions using an SEM Quanta 250™ FEG instrument at 5000 × magnification. The elemental compositions of the LCACs were identified by EuroVector's EA3000 elemental analyzer according to ASTM D5291-96 [42]. The LCACs were analyzed for their Raman spectra using Jasco NRS-4500 spectroscopy suite software. The surface organic functional groups analysis was acquired using a PerkinElmer Spectrum100 Fourier transform infrared spectroscopy (FT-IR) by the KBr method. The thermogravimetric analysis (TGA) of the biomass composition was investigated by the Shimadzu DTG-60H model thermal analyzer starting from 25 up to 600 °C in an inert ambient (heating rate of 10 ºC min^{-1} and flow rate of 50 mL min^{-1}).

Table 1 The KOH impregnation weight ratios (IWR) used and dubbing LCACs

IWR (w/w)	ACs ID
1:2	LCAC2
1:3	LCAC3
1:4	LCAC4

2.4 SGBA assays

Adsorption experiments of benzene were done at 25 and 45 °C, 0 and 80% relative humidity (RH), 1-h contact time with various beginning concentrations (ranging between 10 to 400 mg/L) and 250 mg of LCAC2, LCAC3, and LCAC4 at batch adsorption reactor. Preliminary experiments indicated that this residence time assured the adsorption equilibrium, following the procedure already detailed. After equilibrium concentrations, benzene vapor in the batch reactor was collected rapidly with Tenax®-TA sorbent tubes. It was determined with a chromatography/mass spectrometry detector (GC–MS Thermo Scientific Trace 1300) based on the US EPA TO-17 Method [43]. The equilibrium SGBA capacities were explained with Eq. (1) in which C_i (mg/L) and C_o (mg/L) refer to the benzene content at equilibrium conditions; in addition, the feeder flux rate (F) of 110 mL/min and 250 mg of LCAC2, LCAC3 and LCAC4 (W) were computed for applied adsorption reactions.

$$q_{(mg/g)} = \left(\frac{FxC_0x10^{-9}}{W}\right)\left[\left(\frac{C_i}{C_0}xt_s\right) - \left(\int_0^{t_s}\frac{C_i}{C_0}d_t\right)\right] \quad (1)$$

2.5 Adsorption isotherm models and kinetics

Examining an isotherm is the pivotal step in gaseous adsorption systems design, which connects the benzene molecules and LCAC2, LCAC3, and LCAC4 in the gaseous environment. The MAC of the LCAC2, LCAC3, and LCAC4 were placed to the two non-linear isotherm models, namely Langmuir [44] and Freundlich [45]. The models were applied to describe if either the monolayer adsorption surface containing a limited number of adsorption sites in Eq. (2) is at play or the heterogeneous surface with adsorbent interactions with adsorbed molecules as multilayer adsorption in Eq. (3). The isothermal study shows adsorption equilibrium mechanism regarding the adsorption of benzene onto the LCAC2, LCAC3, and LCAC4.

$$q_e : \frac{q_m x K_L x C_e}{1 + K_L C_e} \quad (2)$$

$$q_e : K_f x C_e^{1/n} \quad (3)$$

where q_m (mg g^{-1}) is a vital variable indicating the MAC for the LCACs used for the remediation of benzene evaporation in the Langmuir model; C_e (mg/L) refers to the equilibrium concentration; K_L (L/mg) is the constant of adsorption equilibrium, which highlights the affinity of adsorption sites of the LCACs (L/mg); K_f (mg/g) is the Freundlich constant, correlated to binding energy, and corresponds to benzene molecules onto the active regions of the LCACs at equilibrium condition of the adsorption step; and n (L g^{-1}) is the parameters of heterogeneity.

To investigate the adsorption kinetic behavior, pseudo first order (PFOM) in Eq. (4) and pseudo second order (PSOM) in Eq. (5). In this work, it was adopted to model kinetic data [46, 47].

$$q_t : q_e(1 - e^{-k_1 t}) \tag{4}$$

$$q_t : \frac{k_2 q_e t}{1 + k_2 q_e t} \tag{5}$$

where k_1 and k_2 are the PFOM unit constant (min^{-1}) and the PSOM rate constant (min^{-1}).

2.6 Thermodynamic study

Thermodynamic variables, including standard enthalpy change (ΔH°, kJ mol^{-1}), standard entropy change (ΔS°, kJ mol^{-1}), and standard Gibbs free energy change (ΔG°, kJ mol^{-1}), are used to investigate the spontaneity, to identify the nature of the mechanism and heat change in the gas adsorption [48]. From the following statements, the parameters can be targeted within Eq. (6)–(9).

$$K_c : C_{Ae}/C_e \tag{6}$$

$$\Delta G^\circ : -\mathrm{RT}\ln K_c \tag{7}$$

$$\Delta G^\circ : \Delta H^\circ - T\Delta S \tag{8}$$

$$\mathrm{Log}K_c : (\Delta S^\circ/2.303R) - (\Delta H^\circ/2.303RT) \tag{9}$$

where C_{Ae} defines the adsorbed benzene onto the LCACs by liter of the reactor at equilibrium (mg/L), R represents the gas constant (8.314 kJ mol^{-1}), T characterizes the temperature (K), and K_c illustrates the equilibrium constant. To obtain ΔH° and ΔS° values, the slope and intercept of the log Kc versus 1/T plot are used. All these findings confirm that the adsorption data are described optimally by the PSOM for the SGBA onto LCACs.

3 Results and discussion

3.1 Textural and morphological characteristics

Determination of the pore structure of LCAC2, LCAC3, and LCAC4 that N_2 adsorption isotherms at − 196 °C gave information of LCACs textural properties using BET equation in Fig. 1 [49]. Sources from the IUPAC [50], LCACs isotherms are clearly type IV, suggesting more mesopores than micropores as the d_p of LCAC2, LCAC3, and LCAC4 are 2.63, 2.52, and 2.19 nm, which is characterized with capillary condensation by the occurrence of a benzene meniscus [51, 52]. Apparently, N_2 uptake enhanced with increased KOH-IWR (1:2, 1:3, 1:4 w/w). The porous texture is formed steadily, and the isotherm type is mainly related to the mesoporous structure (2–50 nm), which LCAC2, LCAC3, and LCAC4 have pronounced H4 hysteresis loop and is connected to capillary condensation occur in the mesopore [53]. Additionally, the preliminary section of the N_2 isotherms has significant N_2 uptake at very low relative pressures ($P/P_0 < 0.01$), favorable for adsorption on microporous ACs [54, 55]. The mesoporosity of LCACs improves because the KOH, as a dehydrating agent, initially interacts with lignin and hemicelluloses to create the mesopore structure [56]. Related results have been described by previous researchers [57, 58].

The elemental composition of LCB, LCAC2, LCAC3, and LCAC4 was characterized, in which the fraction of carbon (C), nitrogen (N), sulfur (S), and hydrogen (H) elements was assessed and oxygen (O) element was measured by the

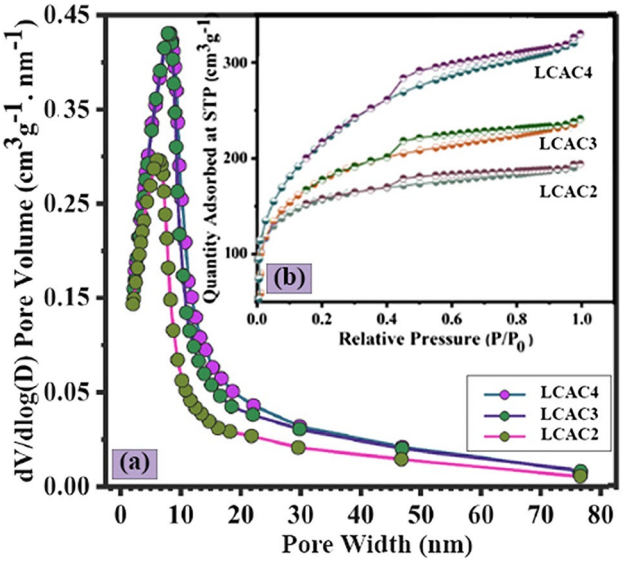

Fig. 1 (a) N_2 adsorption/desorption isotherms at − 196 °C and (b) pore size distribution of LCACs

difference in Table 2. This result shows that ultimate analysis for LCB was 46.3 wt% C, 4.7 wt% H, 0.6 wt% N, 0.8 wt% S, and 47.6 wt% O. The C wt% of LCB increased from 46.3 to 79.1% after activation and carbonization processes, the N wt% increased from 0.6 to 5.8% with the use of carbonization processes, the amount of H wt% was between 2.1 and 4.7% and the sulfur was between 0.8 and 1.9%. There is no clear order, but the decrease in the amount of oxygen from 47.6% to 11.1% is due to the burning of oxygen in the formation of the samples. Analyzing the proximate of LCB was performed using the ASTM D 3172–3175 [6] standard procedure, which contains 14.8 wt% moisture, 54.9 wt% volatile matter, 22.7 wt% fixed carbon, and 7.6 wt% ash.

The use of activation temperature (ACT) accelerates the process of dissolution and thermal degradation of LCACs. This causes an increase in S_{BET} and pore formation in Table 3. The S_{BET} of the LCACs significantly with increasing from 609 to 826 $m^2\ g^{-1}$. The highest S_{BET} of the LCACs is provided at the LCAC4 (ACT at 700 °C and IWR of KOH 1:4 w/w). Numerous researchers present favorable trend outcomes also obtained for the impact of ACT on S_{BET} by KOH activation pretreatment of other feedstocks [59]. For the sake of comparison, S_{BET} and V_{μ} of LCAC2, LCAC3, LCAC4 were 609, 742, and 826 $m^2\ g^{-1}$, 0.237, 0.296, and 0.386 $cm^3\ g^{-1}$. Samiyammal et al. [60] produced CNSAC from cashew nut shell at 600 C by 1:1 and 1:4 w/w KOH and S_{BET} were found to be 297.10 $m^2\ g^{-1}$ and 407.80 $m^2\ g^{-1}$. The S_{BET} of LCACs is higher than CNSAC. The total pore volume (V_T $cm^3\ g^{-1}$) of the LCACs is depicted to increase approximately threefold from 0.321 to 0.454 cm^3/g with increasing both IWR of KOH. The d_p dwindled from 2.63 to 2.19 nm with increasing IWR, and LCACs are mostly microporous, although mesopores are also designed, which is necessary to facilitate the penetration of numerous molecules into the carbon matrix [61]. Similar trends are reported in previous works by Abdel-Ghani et al. [62], Li et al. [63], and Singh et al. [64].

The development of porous LCACs has been mixed with gasification under primary reactions. Also, KOH activation as a pore expander process created a slightly higher porosity [65, 66], while were formed three main stages [67]: (i) gasification of carbon increases porosity and releases H_2O and CO_2, (ii) appearance of the pore skeleton leads to the etching of the carbon skeleton and the formation of K_2O and K_2CO_3, and (iii) formation of metallic K, new pores are formed and existing pores are stretched [68]. Equations (10)–(12) are depicted [69] in three stages, and the formation of K_2O and K_2CO_3 by redox reactions can moderately erode the carbon skeleton when the temperature reaches 700 °C. An important factor here is the presence of a large number of micropores not only on the surface but also in the interior of the carbon, resulting in a hollow and crumbling structure with a high micropore/mesopore ratio at these temperatures [70].

$$2KOH \rightarrow K_2O + H_2O,\ H_2O + C \rightarrow CO + H_2,\ CO + H_2O \rightarrow CO_2 + H_2 \tag{10}$$

$$CO_2 + K_2O \rightarrow K_2CO_3,\ K_2CO_3 \rightarrow K_2O + CO_2,\ CO_2 + C \rightarrow 2CO \tag{11}$$

$$K_2O + 2C \rightarrow K + 2CO,\ \text{and}\ K_2CO_3 + C \rightarrow 2K + 3CO \tag{12}$$

3.2 Surface chemistry properties

Several essential variables can significantly regulate the properties of the porous structure of LCAC2, LCAC3, and LCAC4, such as oxidant concentration, IWR, carbonization temperature, and activation time. Many scholars concluded that the surface chemistry and porosity of AC have a significant effect on its characteristics. In this study, the IWR and the adsorption process to benzene were analyzed repeated three times with a relative standard deviation of less than 10%. Furthermore, the produced AC was thoroughly

Table 2 Elemental and proximate analysis (wt %) of LCB and LCACs

Samples	Elemental analysis					Proximate analysis			
	C	N	H	S	O	Moisture	Volatile matter	Fixed carbon	Ash
LCB	46.3	0.6	4.7	0.8	47.6	14.8	59.9	22.7	2.6
LCAC2	78.2	4.5	2.1	0.7	14.5	8.45	17.03	70.63	3.89
LCAC3	74.9	3.7	4.5	1.9	15	7.68	16.52	71.25	4.55
LCAC4	79.1	5.8	2.8	1.2	11.1	3.37	18.97	73.46	4.20

Table 3 Properties of pore textures of LCACs

Samples	S_{BET} ($m^2\ g^{-1}$)	V_{μ} ($cm^3\ g^{-1}$)	V_m ($cm^3\ g^{-1}$)	V_T ($cm^3\ g^{-1}$)	V_{μ}/V_T (%)	d_p (nm)
LCAC2	609	0.237	0.084	0.321	73.8	2.63
LCAC3	742	0.296	0.091	0.387	76.5	2.52
LCAC4	826	0.386	0.068	0.454	85	2.19

fabricated and characterized using FT-IR, Ramani elemental analysis, SEM, TGA, and N_2 adsorption.

The influence of 1:2, 1:3, and 1:4 (w/w) KOH-IWR at the ACT of 700 °C on the surface functional group is demonstrated by the FT-IR spectra in Fig. 2. LCB, without heat treatment, contains various amounts of volatile and organic compounds. The FT-IR spectrum of LCAC2, LCAC3, and LCAC4 show broadband absorption peaks starting around 3470–3300 cm^{-1} attributed O–H stretching vibration in cellulose, pectin, absorbed water, hemicellulose, and lignin [71, 72] and C–H stretching in alkane, weak peak broadband around 2800 cm^{-1} presents is C–H stretching vibration in the methyl group [73], peaks around 1650–1550 cm^{-1} correspond to the C = C stretching for presence of aromatic or benzene rings in lignin, band at 1350–1000 cm^{-1} can be appointed to C–H stretching of carboxylic acids and alcohols, in the range of 900–600 cm^{-1} indicate diverse bands associated with aromatic, out of plane C = H stretching with numerous degrees of substitution [74]. Similar peaks were reported as ACs porosity and specific surface [75, 76].

The Raman spectra of LCACs revealed that LCAC2, LCAC3, and LCAC4 presented dichotomous D (disorder) and G (graphitization) bands in Fig. 3. The band positions and intensity ratio (I_D/I_G) that defines relative ratio of the irregular structure of turbostratic carbon to ordered graphite crystallites with lower I_D/I_G ratio (LCAC2: 1.09, LCAC3: 1.12, and LCAC4: 0.94) are a reflection of higher aromatic ring structures and less carbon-containing defects [77] that promote the occurrence of surface oxygen functional groups for LCAC2, LCAC3, and LCAC4. However, the existence of both D and G bands in the Raman spectra of LCAC2, LCAC3, and LCAC4 is a recognition of heterogeneous carbon microstructures [78]. In addition, the overlapping of D and G bands in the Raman spectrum of LCAC2, LCAC3, and LCAC4 is evidence of the highly amorphous carbon structures [79]. The D-band locations for LCACs were between 1304 and 1391 cm^{-1}, which is attributed to structural defects. It is not found in perfect graphite, and microstructure occurs in a Raman active mode of approximately 1350 cm^{-1} [80, 81]. This is an indication that the LCACs are not defect-free.

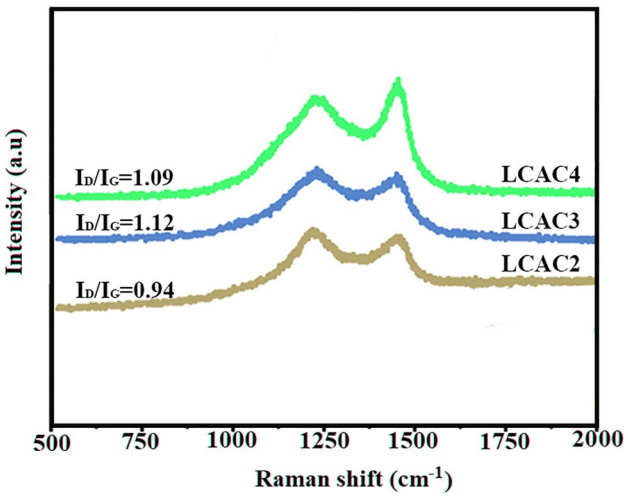

Fig. 3 Raman spectra of LCACs

The thermal stability of the LCB and LCACs was investigated by thermogravimetric analysis (TGA) and presented in Fig. 4. The weight loss stages of LCB, LCAC2, LCAC3, and LCAC4 were observed with increasing temperature. The weight loss value of LCB started at around 200 °C due to its consisting of cellulose, hemicellulose, and lignin. However, total mass loss (predominantly cellulose) of LCAC2,

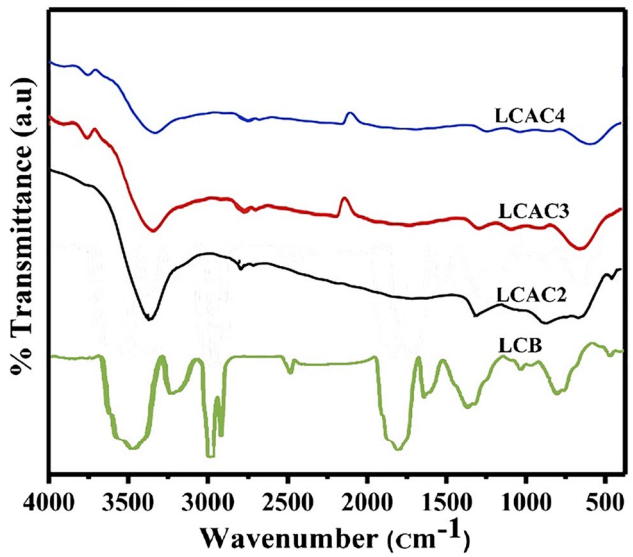

Fig. 2 FT-IR spectra of LCACs

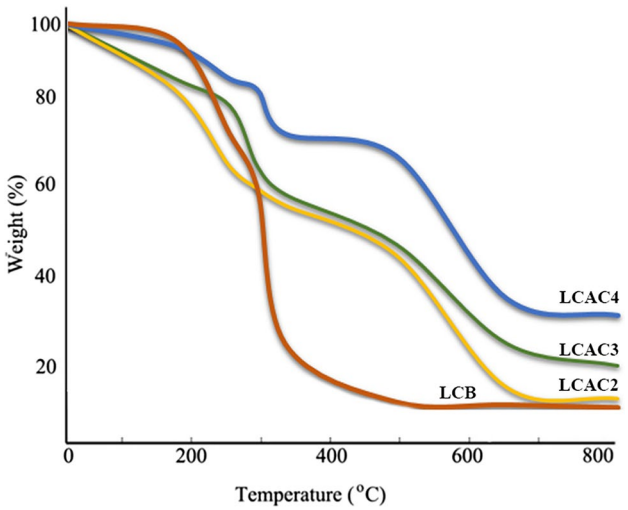

Fig. 4 TGA analyses of LCB and LCACs

LCAC3, and LCAC4 initiated from 370 to 630 °C between 63 and 82 wt%. Compared to cellulose, lignin in biomass usually decomposes at a higher temperature so that the weight staying in the material following the second stage mainly includes lignin decomposition, the formation of carbon structures, and possible inorganic impurities [82].

Scanning electron microscopy (SEM) of the LCACs surface morphology is depicted the surface composition of LCAC2, LCAC3, and LCAC4 in Fig. 5. The result shows that the KOH activation process significantly impacts LCAC porosity and visible variations in the exterior surfaces of the LCACs. A study by Karimnezhad et al. [83] on the preparation of ACs from walnut shells presented that activation with $ZnCl_2$ through chemical activation, compared to IWR of 0.5–2.0 w/w, with increasing IWR caused a successful pore development in ACs. External surfaces have evident spaces that can be caused by the evaporation of KOH during carbonization [84], thus leaving cavities previously filled by the dehydrating agent. LCB image in Fig. 5a, even though there are no voids, no structures, and no pores of any kind, and that in Fig. 5b–d present that the surface of the LCAC2, LCAC3, and LCAC4 is very dense with both large and small pores, curvatures, pores and spongy white spots with occasional cracks in the carbon matrix. As the KOH ratio increases with (1:2 to 1:4 w/w), the S_{BET} increases, as shown in LCAC4, but decreases in LCAC2. In previous literature, it has been shown that evaporation of dehydrating agent previously occupying voids or redundant activation agents still filling the pores of porous carbon has also been demonstrated by Chen et al. [85] and Li et al. [86].

3.3 Mechanism of SGBA onto LCACs

The benzene competitive capacity for LCAC2, LCAC3, and LCAC4 at 25 °C + 0 RH%, 25 °C + 80 RH%, 45 °C + 0 RH% and 45 °C + 80 RH% are given for binary adsorption in Fig. 6. The saturation capacity values of LCAC2, LCAC3, and LCAC4 at 25–45 °C under 0–80 RH% correspond to reductions of 12.9–11.6%, 7.8–11.5%, and 9.9–18.4%. These findings have to take into account the relevant loaded with different amounts. It is considered that the amount of adsorbed benzene molecules increases at the ambient temperature of 45 °C, significantly higher than 25 °C. However, LCACs have the less adsorbed tendency to saturated pore filling under 80 RH% rather than 0 RH% conditions. This is not surprising because investigators were shown to decrease with increasing RH% in the ambient environment and reached equilibrium rapidly at deficient levels [87],

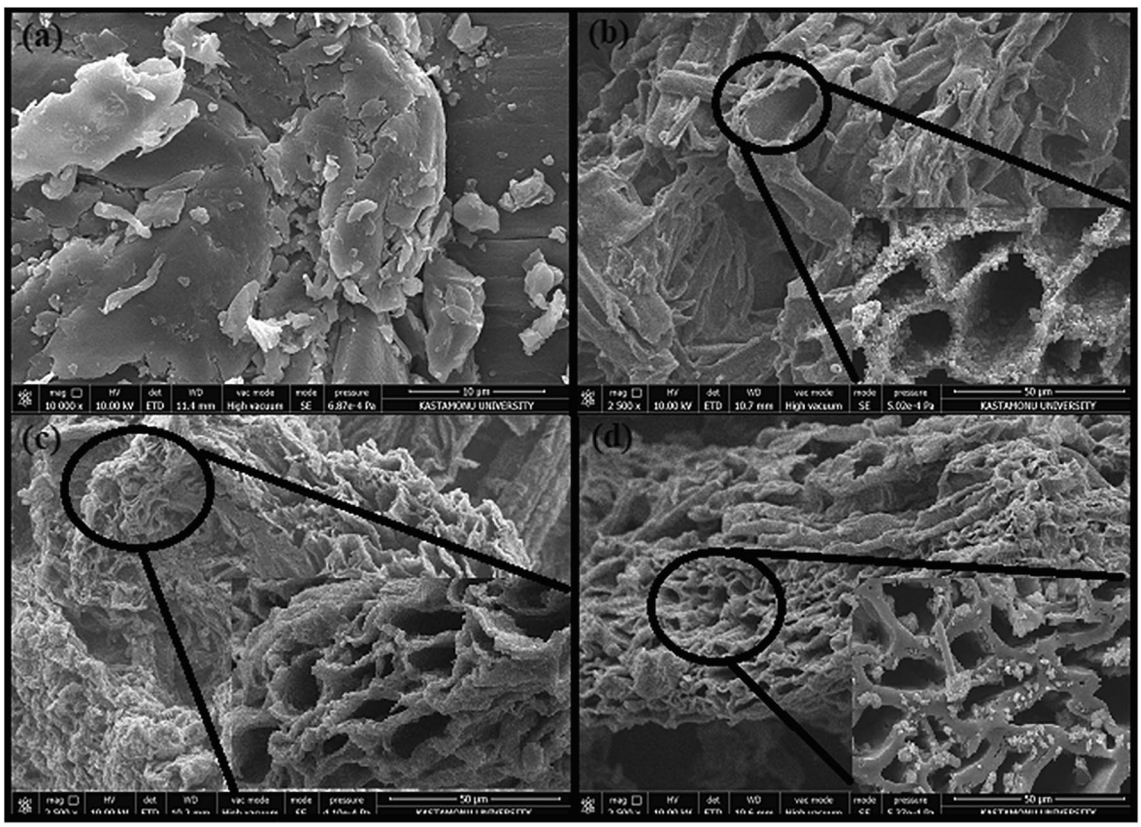

Fig. 5 SEM images **a** LCB, **b** LCAC2, **c** LCAC3, and **d** LCAC4

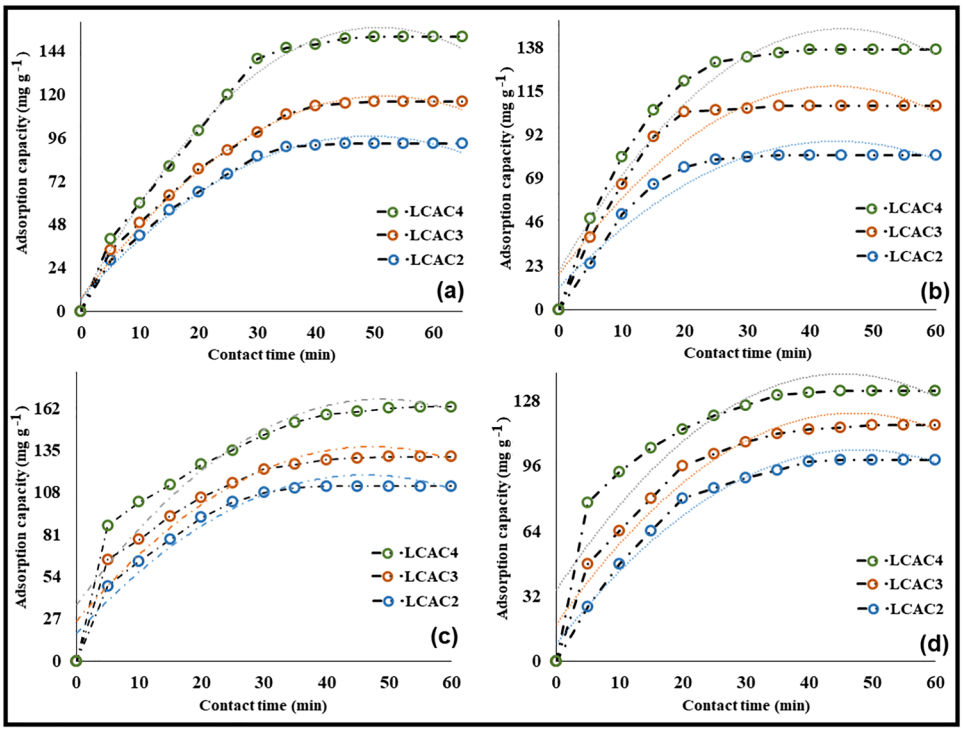

Fig. 6 SGBA capacities of LCACs **a** 25 °C + 0 RH%, **b** 25 °C + 80 RH%, **c** 45 °C + 0 RH%, and **d** 45 °C + 80 RH%

comparing benzene capacity at several conditions, including temperature and humidity conditions represented by [88] and [89].

For steady-state conditions without benzene vapor, including LCAC2, LCAC3, and LCAC4, the experimental setup realized equilibrium adsorption. Experiments were applied to two-parameter Langmuir and Freundlich adsorption isotherms, which were among the best models for fitting the parameters and were investigated in all data sets. The initial concentration values for each kinetics and adsorption equilibrium compound were selected to closely approximate its existence in ambient indoor air in equilibrium and identify which type of conduct of the SGBA mechanism. The Freundlich isotherm, the empirical equivalent, hypothesizes that the sorption reaction occurs on heterogeneous interfaces and that there is no constant number of sites [86, 90]. K_F values are increased, and $1/n$ values are decreased by rising surface temperature, implying that the adsorption capacity and the intensity of adsorption improve with increasing temperature [91, 92]. Also, $1/n$ is a sign of normal Langmuir isotherm ($1/n < 1$) and cooperative adsorption ($1/n > 1$) [93]. Table 4 shows that n values are between 1.30 and 3.92, with relatively high R^2 values (0.93–1.0) compared to Langmuir isotherm's R^2 values (0.75–0.99). The Freundlich isotherm is a convenient option for representing the experimental results of the investigated system under various origin conditions. As is known, temperature appears to be a vital factor in the adsorption mechanism [94]. Their stronger adsorption intensity is achieved through higher temperatures, suggesting an endothermic character.

Table 4 Determined Langmuir and Freundlich non-linear adsorption model parameters onto LCAC4

Conditions	Langmuir			Freundlich		
	q_m (mg g^{-1})	K_L (L/mg)	R^2	n	K_F (mg g^{-1})(L/mg)$^{1/n}$	R^2
10 mg/L, 25 °C, 0 RH%	1.51 ± 1.32	0.173 ± 0.003	0.785 ± 0.003	1.30 ± 0.12	7.416 ± 2.57	0.953 ± 0.022
10 mg/L, 45 °C, 0 RH%	2.08 ± 1.88	0.163 ± 0.002	0.891 ± 0.017	1.316 ± 0.10	9.270 ± 1.93	0.965 ± 0.019
10 mg/L, 25 °C, 80 RH%	43 ± 1.88	0.86 ± 0.036	0.79 ± 0.014	2.30 ± 0.11	37 ± 0.58	0957 ± 0.003
10 mg/L, 45 °C, 80 RH%	47 ± 1.88	0.53 ± 0.058	0.75 ± 0.0013	3.92 ± 0.28	37 ± 0.69	0.931 ± 0.003
400 mg/L, 25 °C, 0 RH%	113 ± 1.88	0.62 ± 0.091	0.97 ± 0.001	1.75 ± 0.34	42 ± 0.27	1 ± 0.000
400 mg/L, 45 °C, 0 RH%	164 ± 1.88	0.19 ± 0.004	0.93 ± 0.001	1.81 ± 0.12	31 ± 0.38	0.96 ± 0.02
400 mg/L, 25 °C, 80 RH%	93 ± 1.88	0.95 ± 0.008	0.99 ± 0.001	1.73 ± 0.53	43 ± 0.57	1 ± 0.01
400 mg/L, 45 °C, 80 RH%	127 ± 1.88	0.63 ± 0.009	0.96 ± 0.003	3.21 ± 0.34	53 ± 0.69	0.98 ± 0.01

3.4 Adsorption kinetics and mechanism

Correlation of adsorption rate with controlling adsorption parameters can be studied by kinetics. The controlling mechanism of benzene for mass transfer and the chemical reaction was examined to fit the pseudo first order (PFOM) and pseudo second order (PSOM). The rate constant (k_1) and correlation coefficient are listed in Table 5. The adsorption kinetics plays an essential role in describing adsorption behavior on the environmental application of the LCAC4, which was applied to kinetic experiments for the highest S_{BET} and V_{μ}. The correlation coefficient for the PSOM kinetic model is 1.000 ± 0.0001, indicating a good PSOM fit to the experimental data.

3.5 Thermodynamic studies

Thermodynamic features of SGBA on LCAC4 were investigated under several conditions for Gibbs free energy ($\Delta G°$, kJ mol^{-1}), enthalpy ($\Delta H°$, kJ mol^{-1}), and entropy ($\Delta S°$, kJ mol^{-1}) by the following equations [95]. Table 6 shows thermodynamic results that the negative values of $\Delta G°$ (from − 21.02 to − 598.77) for all experimented temperatures verify the SGBA onto LCAC4 are thermodynamically possible and inherently [96]; also, $\Delta H°$ values were 60.81 at 25 °C, which is attributed to physical adsorption [97]. The positive values of $\Delta S°$ (from 0.27 to 96.28) indicate the increased randomness at the solid/gas interface during the adsorption of each compound on LCACs. Also, they reflect the affinity of LCAC4 to volatiles. It can be said that the SGBA on LCAC4 is a monolayer physisorption process.

3.6 Regeneration study

Studying the reusability of LCACs for SGBA, five cycles of adsorption–desorption were performed with a sorbent tube filled 400 mg/L benzene with N_2 stream at 200 °C for 2-h and used LCACs as follows: (i) 25 °C + 0 RH%, (ii) 25 °C + 80 RH%, (iii) 45 °C + 0 RH%, and (iv) 45 °C + 80 RH% as given in Fig. 7. The adsorption capacity of LCAC2, LCAC3, and LCAC4 after the treatment at 25 °C + 0 RH%, 25 °C + 80 RH%, 45 °C + 0 RH%, and 45 °C + 80 RH% decreased between Cycle–I and Cycle–V as 93, 116, 152 mg g^{-1} to 40, 56, 82 mg g^{-1}, 81, 107, 137 mg g^{-1} to 15, 38, 42 mg g^{-1}, 112, 131, 163 mg g^{-1} to 66, 60, 80 mg g^{-1}, and 99, 116, 133 mg g^{-1} to 31, 25, 33 mg g^{-1}. LCAC3 also demonstrated a mild downward slope concerning MAC after five cycles of 25–46%. Accordingly, most of the research on the regeneration potential of ACs derived from several carbonaceous feedstocks was observed to recover efficiently after three to five adsorption/regeneration cycles [98, 99]. For instance, Spessato et al. [100] reported that thermal regeneration cycles of the SAC were applied to recover adsorption capacity, which was restored after all cycles for the AC to regain its reusability by 31.92%.

Table 6 Thermodynamic results for SGBA onto LCAC4

Temperature (°C)	$\Delta H°$ (kJ mol^{-1})	$\Delta S°$ (kJ mol^{-1})	$\Delta G°$ (kJ mol^{-1})
25	60.81	0.27	− 21.02
45	2275.96	96.28	− 598.77

4 Conclusions

A comparative analysis of our results revealed that among the synthesized and evaluated three divergent LCACs mesoporous carbons, LCAC4 properties revealed that it is the best adsorbent to capture benzene. The irregularly shaped pores of LCAC4 were investigated for SGBA (10 to 400 mg/L) at different RH (0 and 80%). RH precisely reduced the benzene MAC at low initial benzene concentration compared with dry conditions. The kinetic study of single-component benzene adsorption data on LCAC4 presented that the adsorption rate was controlled mainly by PSOM. The majority of our test conditions favored the

Table 5 Adsorption kinetics model parameters for binary benzene adsorption onto LCAC4

Conditions	q_e, exp (mg g^{-1})	PFOM			PSOM		
		q_e (cal) (mg g^{-1})	k_1 (min^{-1})	R^2	q_e (cal) (mg g^{-1})	k_2 (g/mg/min)	R^2
10 mg/L, 25 °C, 0 RH%	6.423 ± 0.23	1.206 ± 0.05	0.123 ± 0.00	0.869 ± 0.037	5.421 ± 0.02	0.058 ± 0.08	0.998 ± 0.002
10 mg/L, 45 °C, 0 RH%	7.511 ± 0.12	1.222 ± 0.07	0.102 ± 0.003	0.877 ± 0.022	6.602 ± 0.02	0.087 ± 0.05	0.999 ± 0.001
10 mg/L, 25 °C, 80 RH%	6.26 ± 0.19	2.006 ± 0.008	0.059 ± 0.002	0.942 ± 0.037	2.14 ± 0.02	0.075 ± 0.04	0.991 ± 0.002
10 mg/L, 45 °C, 80 RH%	6.31 ± 0.20	2.192 ± 0.00	0.075 ± 0.008	0.932 ± 0.037	2.39 ± 0.02	0.047 ± 0.01	0.984 ± 0.002
400 mg/L, 25 °C, 0 RH%	51.50 ± 0.24	12.731 ± 0.14	0.047 ± 0.008	0.856 ± 0.037	16.46 ± 0.02	0.063 ± 0.06	0.979 ± 0.003
400 mg/L, 45 °C, 0 RH%	74.50 ± 0.36	14.225 ± 0.23	0.063 ± 0.003	0.458 ± 0.037	22.97 ± 0.02	0.075 ± 0.09	0.987 ± 0.004
400 mg/L, 25 °C, 80 RH%	43.40 ± 0.23	10.354 ± 0.25	0.041 ± 0.004	0.569 ± 0.037	18.36 ± 0.02	0.047 ± 0.08	0.994 ± 0.001
400 mg/L, 45 °C, 80 RH%	38.70 ± 0.31	9.852 ± 0.36	0.076 ± 0.005	0.806 ± 0.037	16.83 ± 0.02	0.063 ± 0.04	0.973 ± 0.003

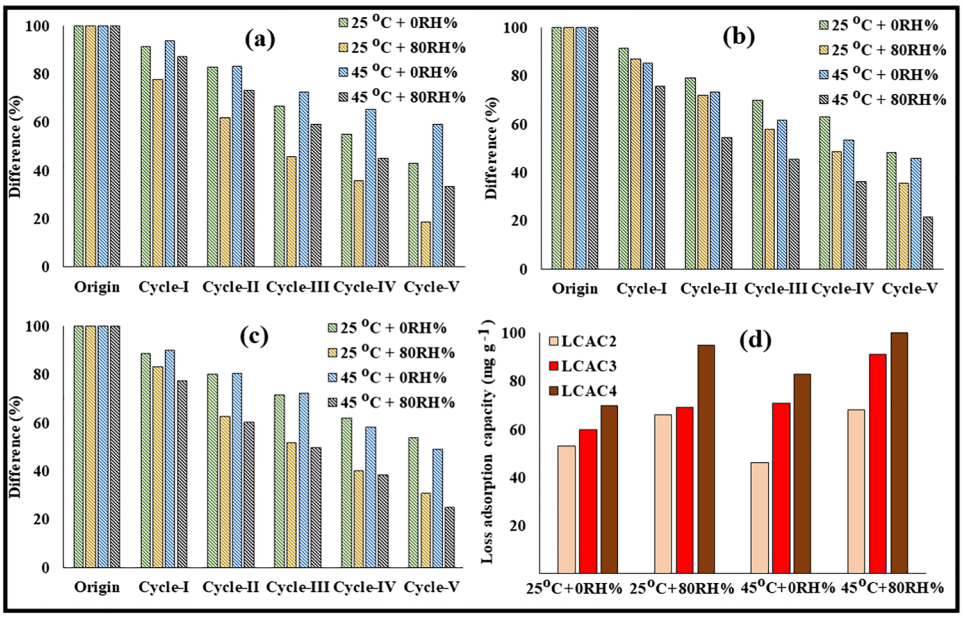

Fig. 7 Adsorption/temperature-swing desorption cycles of **a** LCAC2, **b** LCAC3, **c** LCAC4, and **d** LCACs of towards loss benzene adsorption capacity through several conditions

Freundlich isotherm as a convenient option to simulate the experimental data and spontaneous process involving physical adsorption and exothermic nature at different initial conditions. Temperature-release adsorption/desorption studies for benzene were carried out to investigate the reusability of utilized LCAC4 under various operating conditions. It was observed that benzene adsorption capacity of LCAC4 showed a good performance in dry conditions after five sorption cycles. According to the general conclusions of the present work, LCAC4 has aroused great attention and is a highly appropriate capture adsorbent to abate the emissions of benzene under challenging environmental requirements. It can be exploited to promote improved viability for real-life field situations (ambient pressure, temperature, concentrations, and high humidity) and further experiments for maximizing regeneration must be done.

Author contribution This study is written entirely by Kaan Isinkaralar.

Funding Open access funding provided by the Scientific and Technological Research Council of Türkiye (TÜBİTAK).

Data availability The data that support the findings of this study are available from the corresponding author, upon reasonable request.

Declarations

Ethics approval All authors have read, understood, and have complied as applicable with the statement on "Ethical responsibilities of Authors" as found in the Instructions for Authors.

Consent to participate Not applicable.

Consent for publication Not applicable.

Conflict of interest The authors declare no competing interests.

References

1. Sahu LK (2012) Volatile organic compounds and their measurements in the troposphere. Curr Sci:1645–1649
2. Chin K, Laguerre A, Ramasubramanian P, Pleshakov D, Stephens B, Gall ET (2019) Emerging investigator series: primary emissions, ozone reactivity, and byproduct emissions from building insulation materials. Environ Sci Process Impacts 21(8):1255–1267. https://doi.org/10.1039/C9EM00024K
3. Orecchio S, Fiore M, Barreca S, Vara G (2017) Volatile profiles of emissions from different activities analyzed using canister samplers and gas chromatography-mass spectrometry (GC/MS) analysis: a case study. Int J Environ Res Public Health 14(2):195. https://doi.org/10.3390/ijerph14020195
4. United States Environmental Protection Agency (USEPA) (2011) Volatile organic compounds' impact on indoor air quality. Available online: https://www.epa.gov/indoor-air-quality-iaq/volatile-organic-compounds-impact-indoor-air-quality. Accessed 23 June 2023
5. European Union (1999) VOC-directive: council directive 1999/13/EC of 11 March 1999 on the limitation of emissions of volatile organic compounds due to the use of organic solvents in certain activities and installations. Official Journal of the European Communities, Brussels

6. American Society for Testing and Materials (1999) Annual book of ASTM standards: ASTM
7. World Health Organization (1989) Indoor air quality: organic pollutants. https://doi.org/10.1080/09593338909384805
8. Koppmann R, Von Czapiewski K, Reid JS (2005) A review of biomass burning emissions, part I: gaseous emissions of carbon monoxide, methane, volatile organic compounds, and nitrogen containing compounds. Atmos Chem Phys Discuss 5(5):10455–10516. https://doi.org/10.5194/acpd-5-10455-2005
9. Graedel T (2012) Chemical compounds in the atmosphere. Elsevier
10. ATSDR U (2007) Toxicological profile for lead. US Department of Health and Human Services 1:582
11. IARC Working Group on the Evaluation of Carcinogenic Risks to Humans. List of classifications by cancer sites with sufficient or limited evidence in humans, IARC monographs, volumes 1–132a. Available online: https://monographs.iarc.who.int/wp-content/uploads/2019/07/Classifications_by_cancer_site.pdf. Accessed 24 May 2023
12. Loomis D, Guyton KZ, Grosse Y, El Ghissassi F, Bouvard V, Benbrahim-Tallaa L et al (2017) Carcinogenicity of benzene. Lancet Oncol 18(12):1574–1575. https://doi.org/10.1016/S1470-2045(17)30832-X
13. Hanif NM, Hawari NSSL, Othman M, Abd Hamid HH, Ahamad F, Uning R et al (2021) Ambient volatile organic compounds in tropical environments: potential sources, composition and impacts–a review. Chemosphere 285:131355. https://doi.org/10.1016/j.chemosphere.2021.131355
14. European Commission (2008) Directive 2008/50/EC of the European Parliament and of the council of 21 May 2008 on ambient air quality and cleaner air for Europe. Off J Eur Union 152:1–44
15. Kim HS, Kim HJ, Kim JH, Kim JH, Kang SH, Ryu JH et al (2022) Noble-metal-based catalytic oxidation technology trends for volatile organic compound (VOC) removal. Catalysts 12(1):63. https://doi.org/10.3390/catal12010063
16. Gan G, Fan S, Li X, Zhang Z, Hao Z (2023) Adsorption and membrane separation for removal and recovery of volatile organic compounds. J Environ Sci 123:96–115. https://doi.org/10.1016/j.jes.2022.02.006
17. Bi F, Ma S, Gao B, Liu B, Huang Y, Qiao R, Zhang X (2024) Boosting toluene deep oxidation by tuning metal-support interaction in MOF-derived Pd@ ZrO2 catalysts: the role of interfacial interaction between Pd and ZrO2. Fuel 357:129833. https://doi.org/10.1016/j.fuel.2023.129833
18. Zhang X, Gao B, Rao R, Bi F, Li C, Yue K et al (2024) Defects materials of Institut Lavoisier-125 (Ti) materials enhanced photocatalytic activity for toluene and chlorobenzene mixtures degradation: mechanism study. J Colloid Interface Sci 660:423–439. https://doi.org/10.1016/j.jcis.2024.01.012
19. Adelodun AA (2020) Influence of operation conditions on the performance of non-thermal plasma technology for VOC pollution control. J Ind Eng Chem 92:41–55. https://doi.org/10.1016/j.jiec.2020.08.026
20. Bi F, Wei J, Ma S, Zhao Q, Zhang J, Qiao R et al (2024) Fluorination modification enhanced the water resistance of Universitetet i Oslo-67 for multiple volatile organic compounds adsorption under high humidity conditions: mechanism study. J Colloid Interface Sci 665:898–910. https://doi.org/10.1016/j.jcis.2024.03.192
21. Pradhan S, Parthasarathy P, Mackey HR, Al-Ansari T, McKay G (2024) Food waste biochar: a sustainable solution for agriculture application and soil–water remediation. Carbon Res 3(1):1–29. https://doi.org/10.1007/s44246-024-00123-2
22. Isinkaralar K (2023) Experimental evaluation of benzene adsorption in the gas phase using activated carbon from waste biomass. Biomass Convers Biorefin:1-10. https://doi.org/10.1007/s13399-023-03979-3
23. Zhang M, Sui H, Yang H, Li X, He L, Liu J (2021) Adsorption–desorption behaviors of methanol and ethyl acetate on silica gel: modeling and experimental tests. Ind Eng Chem Res 60(4):1829–1838. https://doi.org/10.1021/acs.iecr.0c05205
24. Ahmadi Y, Kim KH (2023) Recent progress in the development of hyper-cross-linked polymers for adsorption of gaseous volatile organic compounds. Polym Rev 63(2):365–393. https://doi.org/10.1080/15583724.2022.2082470
25. Kim WK, Vikrant K, Younis SA, Kim KH, Heynderickx PM (2023) Metal oxide/activated carbon composites for the reactive adsorption and catalytic oxidation of formaldehyde and toluene in air. J Clean Prod 387:135925. https://doi.org/10.1016/j.jclepro.2023.135925
26. Zhang Q, Han K, Li S, Li M, Li J, Ren K (2018) Synthesis of garlic skin-derived 3D hierarchical porous carbon for high-performance supercapacitors. Nanoscale 10(5):2427–2437. https://doi.org/10.1039/C7NR07158B
27. Fu L, Zuo J, Liao K, Shao M, Si W, Zhang H et al (2023) Preparation of adsorption resin and itas application in VOCs adsorption. J Polym Res 30(5):167. https://doi.org/10.1007/s10965-023-03510-2
28. Khan JH, Marpaung F, Young C, Lin J, Islam MT, Alsheri SM et al (2019) Jute-derived microporous/mesoporous carbon with ultra-high surface area using a chemical activation process. Microporous Mesoporous Mater 274:251–256. https://doi.org/10.1016/j.micromeso.2018.07.050
29. Kyzas GZ, McKay G, Al-Musawi TJ, Salehi S, Balarak D (2022) Removal of benzene and toluene from synthetic wastewater by adsorption onto magnetic zeolitic imidazole framework nanocomposites. Nanomaterials 12(17):3049. https://doi.org/10.3390/nano12173049
30. Sudhan N, Subramani K, Karnan M, Ilayaraja N, Sathish M (2017) Biomass-derived activated porous carbon from rice straw for a high-energy symmetric supercapacitor in aqueous and non-aqueous electrolytes. Energy Fuel 31(1):977–985. https://doi.org/10.1021/acs.energyfuels.6b01829
31. Kim WK, Younis SA, Kim KH (2022b) The control on adsorption kinetics and selectivity of formaldehyde in relation to different surface-modification approaches for microporous carbon bed systems. Sep Purif Technol 283:120178. https://doi.org/10.1016/j.seppur.2021.120178
32. Shen Q, Lu Z, Bi F, Zhang D, Li L, Zhang X et al (2023) Regulating electronic metal-support interaction by synthetic methods to enhance the toluene degradation over Pt/Co3O4 catalysts. Sep Purif Technol 325:124707. https://doi.org/10.1016/j.seppur.2023.124707
33. Khararoodi MG, Lee CS, Haghighat F (2022) Modelling of sorbent-based gas filters for indoor environment: a comprehensive review. Build Environ 208:108579. https://doi.org/10.1016/j.buildenv.2021.108579
34. Zhang X, Rao R, Gao B, Ma S, Bi F, Li C et al (2023) Crystal engineering of TiO2 enhanced photothermal catalytic degradation of DEHP on Pt catalysts. Mater Today Chem 34:101755. https://doi.org/10.1016/j.mtchem.2023.101755
35. Ma X, Yang L, Hou Y, Zhou L (2022) Adsorption/desorption characteristics of low-concentration semi-volatile organic compounds in vapor phase on activated carbon. J Environ Manag 305:114360. https://doi.org/10.1016/j.jenvman.2021.114360
36. Ha SH, Younis SA, Vikrant K, Szulejko JE, Kim KH (2022) Evidence of the dominant role of particle size in controlling the dynamic adsorption breakthrough behavior of gaseous benzene

in a microporous carbon bed system. Chem Eng J 427:130977. https://doi.org/10.1016/j.cej.2021.130977
37. Wei Q, Chen Z, Cheng Y, Wang X, Yang X, Wang Z (2019) Preparation and electrochemical performance of orange peel based-activated carbons activated by different activators. Colloids Surf A Physicochem Eng Asp 574:221–227. https://doi.org/10.1016/j.colsurfa.2019.04.065
38. Oueslati K, Naifar A, Sakly A, Kyzas GZ, Lamine AB (2022) Statistical and physical interpretation of dye adsorption onto low-cost biomass by using simulation methods. Colloids Surf A Physicochem Eng Asp 646:128969. https://doi.org/10.1016/j.colsurfa.2022.128969
39. Vargas DP, Giraldo L, Silvestre-Albero J, Moreno-Piraján JC (2011) CO 2 adsorption on binderless activated carbon monoliths. Adsorption 17:497–504. https://doi.org/10.1007/s10450-010-9309-z
40. Palodkar AV, Anupam K, Roy Z, Saha BB, Halder GN (2017) High pressure adsorption isotherms of nitrogen onto granular activated carbon for a single bed pressure swing adsorption refrigeration system. Heat Mass Transf 53:3155–3166. https://doi.org/10.1007/s00231-017-2057-9
41. Villarroel-Rocha J, Barrera D, Sapag K (2014) Introducing a self-consistent test and the corresponding modification in the Barrett, Joyner and Halenda method for pore-size determination. Microporous Mesoporous Mater 200:68–78. https://doi.org/10.1016/j.micromeso.2014.08.017
42. Ahmed N, Zeeshan M, Iqbal N, Farooq MZ, Shah SA (2018) Investigation on bio-oil yield and quality with scrap tire addition in sugarcane bagasse pyrolysis. J Clean Prod 196:927–934. https://doi.org/10.1016/j.jclepro.2018.06.142
43. US Environmental Protection Agency (1999) Compendium Method TO-17 determination of volatile organic compounds in ambient air using active sampling onto sorbent tubes. U.S. EPA Technical Assistance Document. EPA/625/R-96/010b
44. Langmuir I (1918) The adsorption of gases on plane surfaces of glass, mica and platinum. J Am Chem Soc 40(9):1361–1403. https://doi.org/10.1021/ja02242a004
45. Freundlich HMF (1906) Over the adsorption in solution. J Phys Chem 57(385471):1100–1107
46. Norouzi S, Heidari M, Alipour V, Rahmanian O, Fazlzadeh M, Mohammadi-Moghadam F et al (2018) Preparation, characterization and Cr (VI) adsorption evaluation of NaOH-activated carbon produced from date press cake; an agro-industrial waste. Bioresour Technol 258:48–56. https://doi.org/10.1016/j.biortech.2018.02.106
47. Alwared AI, Al-Musawi TJ, Muhaisn LF, Mohammed AA (2021) The biosorption of reactive red dye onto orange peel waste: a study on the isotherm and kinetic processes and sensitivity analysis using the artificial neural network approach. Environ Sci Pollut Res 28:2848–2859. https://doi.org/10.1007/s11356-020-10613-6
48. Lima EC, Hosseini-Bandegharaei A, Moreno-Piraján JC, Anastopoulos I (2019) A critical review of the estimation of the thermodynamic parameters on adsorption equilibria. Wrong use of equilibrium constant in the Van't Hoof equation for calculation of thermodynamic parameters of adsorption. J Mol Liq 273:425–434. https://doi.org/10.1016/j.molliq.2018.10.048
49. Brunauer S, Emmett PH, Teller E (1938) Adsorption of gases in multimolecular layers. J Am Chem Soc 60(2):309–319. https://doi.org/10.1021/ja01269a023
50. IUPAC (1972) Manual of symbols and terminology for physicochemical quantities and units. Butterworths, London
51. Rouquerol J, Rouquerol F, Llewellyn P, Maurin G, Sing K (2013) Adsorption by powders and porous solids: principles, methodology and applications. Academic press
52. Jaria G, Silva CP, Oliveira JA, Santos SM, Gil MV, Otero M et al (2019) Production of highly efficient activated carbons from industrial wastes for the removal of pharmaceuticals from water—a full factorial design. J Hazard Mater 370:212–218. https://doi.org/10.1016/j.jhazmat.2018.02.053
53. Liu Z, Sun Y, Xu X, Meng X, Qu J, Wang Z et al (2020) Preparation, characterization and application of activated carbon from corn cob by KOH activation for removal of hg (II) from aqueous solution. Bioresour Technol 306:123154. https://doi.org/10.1016/j.biortech.2020.123154
54. Ponomarev N, Sillanpää M (2019) Combined chemical-templated activation of hydrolytic lignin for producing porous carbon. Ind Crop Prod 135:30–38. https://doi.org/10.1016/j.indcrop.2019.03.050
55. Al-Musawi TJ, McKay G, Kadhim A, Joybari MM, Balarak D (2024) Activated carbon prepared from hazelnut shell waste and magnetized by Fe3O4 nanoparticles for highly efficient adsorption of fluoride. Biomass Convers Biorefinery 14(4):4687–4702. https://doi.org/10.1007/s13399-022-02593-z
56. Mechati F, Bouchelta C, Medjram MS, Benrabaa R, Ammouchi N (2015) Effect of hard and soft structure of different biomasses on the porosity development of activated carbon prepared under N2/microwave radiations. J Environ Chem Eng 3(3):1928–1938. https://doi.org/10.1016/j.jece.2015.07.007
57. Tian X, Ma H, Li Z, Yan S, Ma L, Yu F et al (2017) Flute type micropores activated carbon from cotton stalk for high performance supercapacitors. J Power Sources 359:88–96. https://doi.org/10.1016/j.jpowsour.2017.05.054
58. Wei H, Chen J, Fu N, Chen H, Lin H, Han S (2018) Biomass-derived nitrogen-doped porous carbon with superior capacitive performance and high CO2 capture capacity. Electrochim Acta 266:161–169. https://doi.org/10.1016/j.electacta.2017.12.192
59. Nam H, Wang S, Jeong HR (2018) TMA and H2S gas removals using metal loaded on rice husk activated carbon for indoor air purification. Fuel 213:186–194. https://doi.org/10.1016/j.fuel.2017.10.089
60. Samiyammal P, Kokila A, Pragasan LA, Rajagopal R, Sathya R, Ragupathy S et al (2022) Adsorption of brilliant green dye onto activated carbon prepared from cashew nut shell by KOH activation: studies on equilibrium isotherm. Environ Res 212:113497. https://doi.org/10.1016/j.envres.2022.113497
61. Pallarés J, González-Cencerrado A, Arauzo I (2018) Production and characterization of activated carbon from barley straw by physical activation with carbon dioxide and steam. Biomass Bioenergy 115:64–73. https://doi.org/10.1016/j.biombioe.2018.04.015
62. Abdel-Ghani NT, El-Chaghaby GA, ElGammal MH, Rawash ESA (2016) Optimizing the preparation conditions of activated carbons from olive cake using KOH activation. New Carb Mater 31(5):492–500. https://doi.org/10.1016/S1872-5805(16)60027-6
63. Li S, Han K, Li J, Li M, Lu C (2017) Preparation and characterization of super activated carbon produced from gulfweed by KOH activation. Microporous Mesoporous Mater 243:291–300. https://doi.org/10.1016/j.micromeso.2017.02.052
64. Singh J, Bhunia H, Basu S (2019) Adsorption of CO2 on KOH activated carbon adsorbents: effect of different mass ratios. J Environ Manag 250:109457. https://doi.org/10.1016/j.jenvman.2019.109457
65. Hui TS, Zaini MAA (2015) Potassium hydroxide activation of activated carbon: a commentary. Carbon Lett 16(4):275–280. https://doi.org/10.5714/CL.2015.16.4.275
66. Oginni O, Singh K, Oporto G, Dawson-Andoh B, McDonald L, Sabolsky E (2019) Influence of one-step and two-step KOH activation on activated carbon characteristics. Bioresour Technol Rep 7:100266. https://doi.org/10.1016/j.biteb.2019.100266

67. Wang B, Qiu J, Feng H, Sakai E, Komiyama T (2016) KOH-activated nitrogen doped porous carbon nanowires with superior performance in supercapacitors. Electrochim Acta 190:229–239. https://doi.org/10.1016/j.electacta.2016.01.038
68. Chiang YC, Juang RS (2017) Surface modifications of carbonaceous materials for carbon dioxide adsorption: a review. J Taiwan Inst Chem Eng 71:214–234. https://doi.org/10.1016/j.jtice.2016.12.014
69. Xu Z, Chen J, Zhang X, Song Q, Wu J, Ding L et al (2019) Template-free preparation of nitrogen-doped activated carbon with porous architecture for high-performance supercapacitors. Microporous Mesoporous Mater 276:280–291. https://doi.org/10.1016/j.micromeso.2018.09.023
70. Otowa T, Tanibata R, Itoh M (1993) Production and adsorption characteristics of MAXSORB: high-surface-area active carbon. Gas Sep Purif 7(4):241–245. https://doi.org/10.1016/0950-4214(93)80024-Q
71. Sevilla M, Maciá-Agulló JA, Fuertes AB (2011) Hydrothermal carbonization of biomass as a route for the sequestration of CO2: chemical and structural properties of the carbonized products. Biomass Bioenergy 35(7):3152–3159. https://doi.org/10.1016/j.biombioe.2011.04.032
72. Reddy JP, Rhim JW (2014) Isolation and characterization of cellulose nanocrystals from garlic skin. Mater Lett 129:20–23. https://doi.org/10.1016/j.matlet.2014.05.019
73. Mishra S, Yadav SS, Rawat S, Singh J, Koduru JR (2019) Corn husk derived magnetized activated carbon for the removal of phenol and para-nitrophenol from aqueous solution: interaction mechanism, insights on adsorbent characteristics, and isothermal, kinetic and thermodynamic properties. J Environ Manag 246:362–373. https://doi.org/10.1016/j.jenvman.2019.06.013
74. Li M, Li W, Liu S (2011) Hydrothermal synthesis, characterization, and KOH activation of carbon spheres from glucose. Carbohydr Res 346(8):999–1004. https://doi.org/10.1016/j.carres.2011.03.020
75. Jawad AH, Abdulhameed AS (2020) Statistical modeling of methylene blue dye adsorption by high surface area mesoporous activated carbon from bamboo chip using KOH-assisted thermal activation. Energy Ecol Environ 5(6):456–469. https://doi.org/10.1007/s40974-020-00177-z
76. Bashir T, Dutta J, Masarat S, Kyzas GZ (2024) Formulation and characterization of lignin modified chitosan beads. Adsorption:1–9. https://doi.org/10.1007/s10450-024-00478-3
77. Cai J, Qi J, Yang C, Zhao X (2014) Poly (vinylidene chloride)-based carbon with ultrahigh microporosity and outstanding performance for CH4 and H2 storage and CO2 capture. ACS Appl Mater Interfaces 6(5):3703–3711. https://doi.org/10.1021/am500037b
78. Tee E, Tallo I, Kurig H, Thomberg T, Jänes A, Lust E (2015) Huge enhancement of energy storage capacity and power density of supercapacitors based on the carbon dioxide activated microporous SiC-CDC. Electrochim Acta 161:364–370. https://doi.org/10.1016/j.electacta.2015.02.106
79. Ochai-Ejeh FO, Bello A, Dangbegnon J, Khaleed AA, Madito MJ, Bazegar F, Manyala N (2017) High electrochemical performance of hierarchical porous activated carbon derived from lightweight cork (Quercus suber). J Mater Sci 52:10600–10613. https://doi.org/10.1007/s10853-017-1205-4
80. Bedin KC, Martins AC, Cazetta AL, Pezoti O, Almeida VC (2016) KOH-activated carbon prepared from sucrose spherical carbon: adsorption equilibrium, kinetic and thermodynamic studies for methylene blue removal. Chem Eng J 286:476–484. https://doi.org/10.1016/j.cej.2015.10.099
81. Karakehya N (2023) Effects of one-step and two-step KOH activation method on the properties and supercapacitor performance of highly porous activated carbons prepared from Lycopodium clavatum spores. Diam Relat Mater 135:109873. https://doi.org/10.1016/j.diamond.2023.109873
82. Wang H, Pu Y, Ragauskas A, Yang B (2019) From lignin to valuable products–strategies, challenges, and prospects. Bioresour Technol 271:449–461. https://doi.org/10.1016/j.biortech.2018.09.072
83. Karimnezhad L, Haghighi M, Fatehifar E (2014) Adsorption of benzene and toluene from waste gas using activated carbon activated by ZnCl 2. Front Env Sci Eng 8:835–844. https://doi.org/10.1007/s11783-014-0695-4
84. Borghei SA, Zare MH, Ahmadi M, Sadeghi MH, Marjani A, Shirazian S, Ghadiri M (2021) Synthesis of multi-application activated carbon from oak seeds by KOH activation for methylene blue adsorption and electrochemical supercapacitor electrode. Arab J Chem 14(2):102958. https://doi.org/10.1016/j.arabjc.2020.102958
85. Chen R, Li L, Liu Z, Lu M, Wang C, Li H et al (2017) Preparation and characterization of activated carbons from tobacco stem by chemical activation. J Air Waste Manage Assoc 67(6):713–724. https://doi.org/10.1080/10962247.2017.1280560
86. Li Z, Gao X, Wu L, Wang K, Kobayashi N (2017) Preparation of activated carbons from poplar wood by chemical activation with KOH. J Porous Mater 24:193–202. https://doi.org/10.1007/s10934-016-0252-6
87. Alyasi H, Mackey H, McKay G (2023) Adsorption of methyl Orange from water using chitosan bead-like materials. Molecules 28(18):6561. https://doi.org/10.3390/molecules28186561
88. Huang GG, Liu YF, Wu XX, Cai JJ (2019) Activated carbons prepared by the KOH activation of a hydrochar from garlic peel and their CO2 adsorption performance. New Carbon Mater 34(3):247–257. https://doi.org/10.1016/S1872-5805(19)60014-4
89. Isinkaralar K (2023) Optimal preparation of low-cost activated carbon: the enhanced mechanism of interaction and performance studies for volatile organic compounds (VOCs) capture. Biomass Convers Biorefin:1–10. https://doi.org/10.1007/s13399-023-05159-9
90. Zhang S, Yao L, Xu B, Yang L, Dai Z, Jiang W (2024) Recent advances in zeolite-based materials for volatile organic compounds adsorption. Sep Purif Technol:127742. https://doi.org/10.1016/j.seppur.2024.127742
91. Isinkaralar K (2022) High-efficiency removal of benzene vapor using activated carbon from Althaea officinalis L. biomass as a lignocellulosic precursor. Environ Sci Pollut Res 29(44):66728–66740. https://doi.org/10.1007/s11356-022-20579-2
92. Kouvalakidou SL, Varoutoglou A, Alibrahim KA, Alodhayb AN, Mitropoulos AC, Kyzas GZ (2023) Batch adsorption study in liquid phase under agitation, rotation, and nanobubbles: comparisons in a multi-parametric study. Environ Sci Pollut Res 30(53):114032–114043. https://doi.org/10.1007/s11356-023-30342-w
93. Tiwari AK, Sen D, Das A, Bahadur J (2023) Evidence of size stratification in colloidal glass microgranules realized by rapid evaporative assembly. Langmuir 39(44):15572–15586. https://doi.org/10.1021/acs.langmuir.3c01872
94. Mariyam S, Parthasarathy P, Pradhan S, Al-Ansari T, McKay G (2024) Co-pyrolysis of biomass and binary single-use plastics: synergy, kinetics, and thermodynamics. Int J Sustain Energy 43(1):2168003. https://doi.org/10.1080/14786451.2023.2168003
95. Peydayesh M, Rahbar-Kelishami A (2015) Adsorption of methylene blue onto Platanus orientalis leaf powder: kinetic, equilibrium and thermodynamic studies. J Ind Eng Chem 21:1014–1019. https://doi.org/10.1016/j.jiec.2014.05.010
96. Du X, Guang W, Cheng Y, Hou Z, Liu Z, Yin H et al (2020) Thermodynamics analysis of the adsorption of CH4 and CO2 on montmorillonite. Appl Clay Sci 192:105631. https://doi.org/10.1016/j.clay.2020.105631
97. Elmiz M, Essifi K, Berraaouan D, Salhi S, Tahani A (2019) Adsorption thermodynamics and isosteric heat of adsorption

of thymol onto sodic, pillared and organic bentonite. Mediterr J Chemi 8(6):494–504. https://doi.org/10.13171/mjc8619080210em
98. Araga R, Soni S, Sharma CS (2017) Fluoride adsorption from aqueous solution using activated carbon obtained from KOH-treated jamun (Syzygium cumini) seed. J Environ Chem Eng 5(6):5608–5616. https://doi.org/10.1016/j.jece.2017.10.023
99. Srivastava A, Gupta B, Majumder A, Gupta AK, Nimbhorkar SK (2021) A comprehensive review on the synthesis, performance, modifications, and regeneration of activated carbon for the adsorptive removal of various water pollutants. J Environ Chem Eng 9(5):106177. https://doi.org/10.1016/j.jece.2021.106177
100. Spessato L, Bedin KC, Cazetta AL, Souza IP, Duarte VA, Crespo LH et al (2019) KOH-super activated carbon from biomass waste: insights into the paracetamol adsorption mechanism and thermal regeneration cycles. J Hazard Mater 371:499–505. https://doi.org/10.1016/j.jhazmat.2019.02.102